Journal of Power Sources, *10* (1983) 343 - 354

INVESTIGATION OF POSITIVE ELECTRODE CHARACTERISTICS IN HIGH RATE $Li/SOCl_2$ CELLS

S. SZPAK

Naval Ocean Systems Center, San Diego, CA 92152 (U.S.A.)

J. R. DRISCOLL

Altus Corporation, San Jose, CA 95112 (U.S.A.)

(Accepted June 20, 1983)

Summary

Operational characteristics of the positive electrode in high discharge rate $Li/SOCl_2$ batteries (with $i > 60$ mA cm^{-2}) are investigated using the voltage–current relations augmented by scanning electron microscopy (SEM) and energy dispersive X-ray analysis (EDAX) examination of discharged cathodes. It is shown that the pore volume is an important parameter and that provisions for the expansion of the electrode matrix must be incorporated for full capacity utilization. Cathode additives are most effective at moderate rates, becoming less so as the discharge rate is increased. Both electrochemical and non-electrochemical processes participate in the termination of battery operation and their effect must be considered while formulating and designing the positive electrode for a high rate performance.

Introduction

The development and construction of $Li/SOCl_2$ batteries operating at high power levels have only recently been undertaken. To achieve high discharge rate, defined as power output per unit volume rather than in terms of rate of charge transfer reaction, two design approaches are available: thin cell construction, and flowing electrolyte.

In the majority of $Li/SOCl_2$ cells, the reduction of $SOCl_2$ takes place on Teflon bonded carbon surfaces. The relationship between the electrode structure and performance was studied theoretically by Marincic [1] and experimentally, among others, by Dey [2] and Christopulos and Gilman [3]. These studies revealed that pore volume is one of the relevant factors.

Dey's, and Christopoulos and Gilman's work indicate that consideration of mass transport should be included even at low discharge rates. As the discharge rates are increased, the structural characteristics of the electrode matrix as well as the physico-chemical properties, particularly transport prop-

0378-7753/83/$3.00

erties, of the electrolyte are expected to play an increasingly significant role. This was confirmed, in part, by the results of Klinedinst and Domeniconi [4] and those of Bro and Dey [5] where cathode utilization was found to decrease with increased discharge rate.

The purpose of this communication is to examine in some detail the behavior of porous electrodes employed in high discharge rate $Li/SOCl_2$ cells, and to indicate which of the design parameters most affect their performance. Our discussion is limited to the reserve type, static electrolyte, thin cell configuration. Conclusions are based on the analysis of the voltage–time curves, *i.e.*, on the analysis of the behavior of cells discharged at constant load. These analyses are augmented by the scanning electron microscope (SEM) and energy dispersive X-ray analysis (EDAX) examination of spent electrodes to indicate reasons for the termination of the discharge process for a given set of operating conditions.

Practical carbon electrodes

The fabrication of practical electrodes is, as a rule, protected by patent rights and guarded as proprietary information. The most common matrix of practical electrodes is Teflon bonded Shawinigan black containing various additives such as dispersed copper [6], platinum [7] and iron or cobalt phthalocyanines [8]. Our discussion here is limited to electrodes containing 20 wt.% metallic copper dispersed throughout the Teflon bonded Shawinigan black matrix [6]. We believe, however, that observations reported here, and the conclusions reached, are applicable to other compositions and methods of fabrication.

Figure 1 is an SEM photograph of the cross section of a fresh, Cu containing, Shawinigan black electrode matrix. The distribution of Cu particles

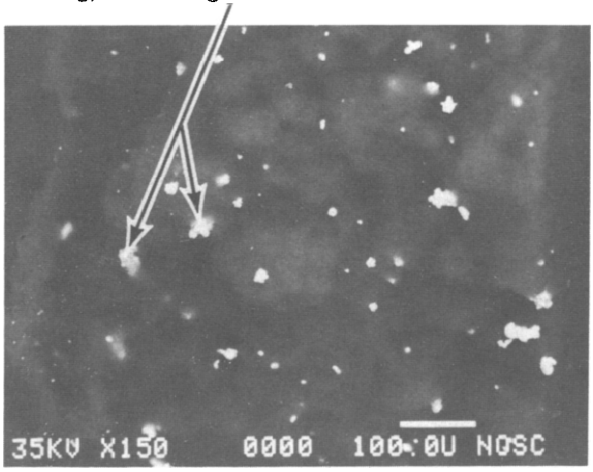

Fig. 1. Cross section of Cu-containing Shawinigan black electrode matrix. Arrows indicate clusters of Cu particles.

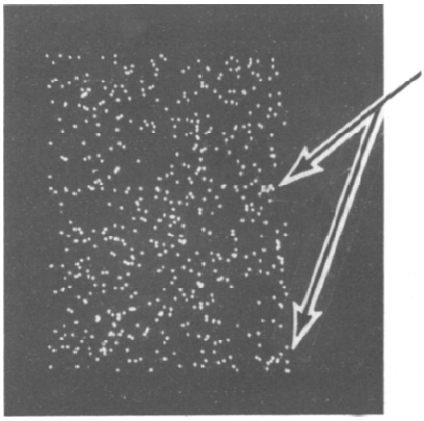

Fig. 2. Computer generated random distribution of particles. Cluster formation indicated by arrows.

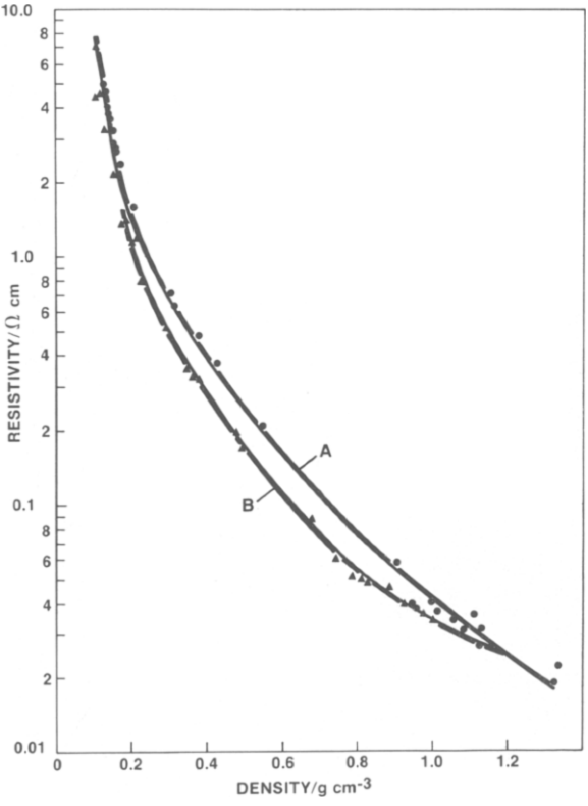

Fig. 3. Electrical resistance as function of electrode matrix density. Curve A, without dispersed copper; curve B, with 20 wt.% copper added.

(20 - 30 μm) is highlighted by operating the SEM in the compositional mode. Evidently, some of the particles are clustered together and surrounded by compacted carbon particles of submicron size. Such a cluster formation is a random process since computer simulation reveals similar cluster formation from a random removal of perfectly arranged spheres, as demonstrated in Fig. 2.

The addition of Cu does not significantly increase the electrode matrix conductivity (Fig. 3). This is in contrast to an earlier report that the electrical conductivity of a mix of conducting and non-conducting spheres of approximately the same size exhibits a sharp transition from non-conducting to conducting at 18 vol.% of metallic constituent [9]. The reason for this is seen in Fig. 4. Here, large Cu particles mixed with only 10% carbon black are completely covered with a thin layer of carbon. Upon compacting, the carbon network is maintained, leaving the matrix conductivity unchanged, Fig. 5.

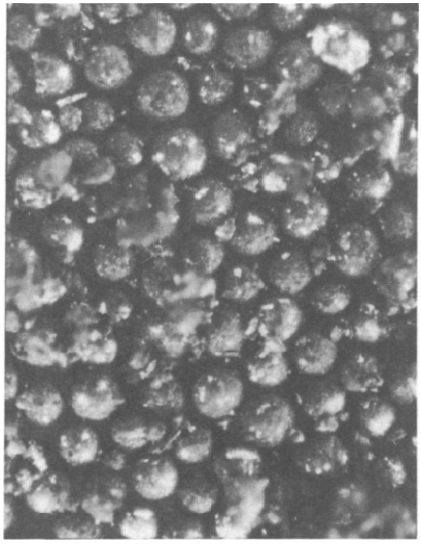

Fig. 4. Thin layer of Shawinigan black deposited on large Cu spheres by mixing (Cu/C ratio 9/1).

Fig. 5. Retention of continuous carbon network upon compression.

Voltage–time curves

Results reported by Dey [2], Christopulos and Gilman [3] and, particularly by Bro and Dey [5], would suggest that the cathode capacity is limited

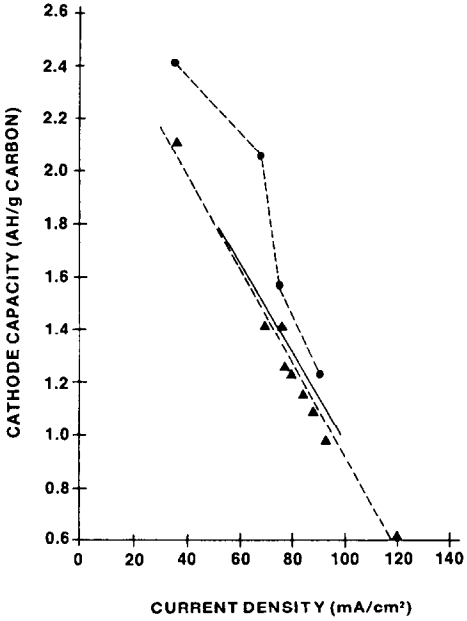

Fig. 6. Effect of electrode porosity on cathode capacity as function of discharge current density; —▲—▲—, production cathodes, single cell data; ——, production cathodes, multiple stack data; —●—●—, development cathodes, single cell data. Electrolyte, 1.9M $LiAlCl_4$ + 0.3M $AlCl_3$ in $SOCl_2$. Temperature, room.

by the amount of $SOCl_2$ stored within the pore volume. This implies that there is no substantial transport of material from the separator to the electrode matrix. Results summarized in Fig. 6 support this conclusion. The upper curve demonstrates the effect of an increase in pore volume on electrode capacity. It is seen that at current densities less than 60 mA/cm^2 the effect is substantial. It is within this regime of operation that the cathode additives are expected to play a major role, irrespective of whether they affect the electrochemical or non-electrochemical elementary processes.

The role of Cu and other additives in the electrochemical reduction of $SOCl_2$ has not been definitively established. In the case of Cu, arguments have been offered that the Cu^{2+}/Cu^{+} couple is involved [10]. Other additives, such as dispersed Pt or Co- and/or Fe-phthalocyanine, may be effective in reducing cell polarization by a mechanism similar to the reduction of oxygen [11, 12].

The modification of electrode composition is expected to be most effective at moderate discharge rates, where the kinetic restrictions overshadow the mass transport limitations. At higher current densities, this effect is expected to be less because the transition from kinetic to transport control of electrochemical or non-electrochemical processes should become dominant. Under these conditions the termination of electrode operation may be attributed to either depletion of active material or, alternatively, to blockage of electrode structure by precipitation of LiCl.

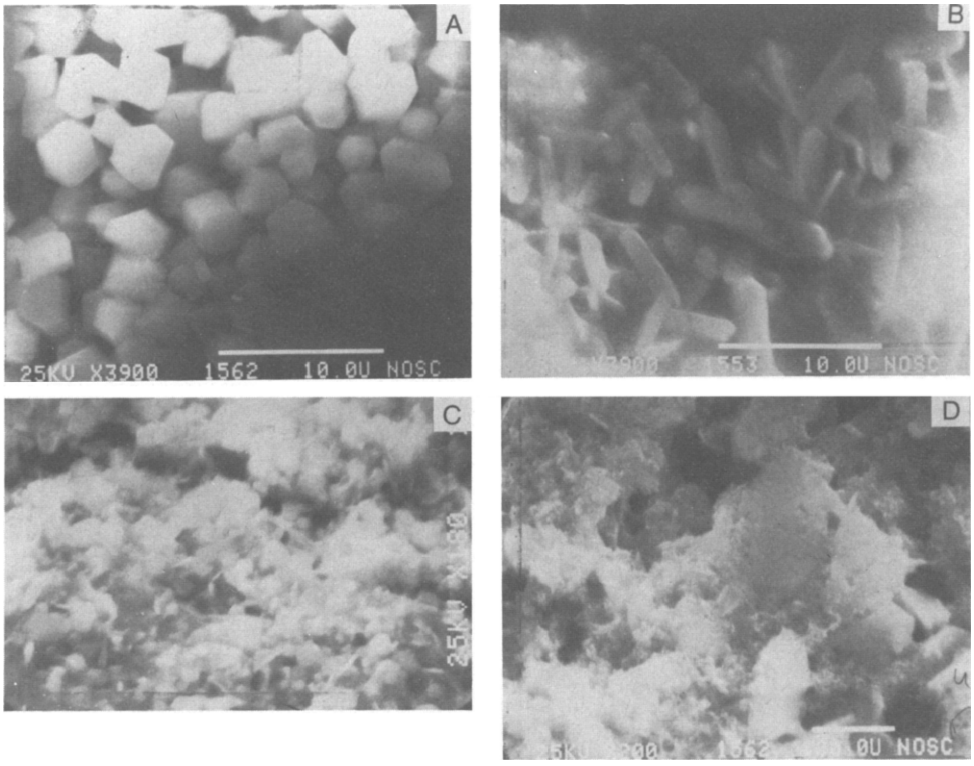

Fig. 7. Growth forms of LiCl crystallites. A, well defined cubic crystallites; B, elongated, plate-like growth; C, elongated, plate-like crystallites resting upon larger cubic crystallites; D, fused crystallites indicating mechanically restricted growth form. Electrolyte, 1.9M $LiAlCl_4$ + 0.3M $AlCl_3$ in $SOCl_2$. Temperature, room.

Reaction product morphology

In practical electrodes, the reduction of $SOCl_2$ occurs within the confines of a porous structure. As the reaction proceeds and the $SOCl_2$ solvent is used up, the solubility of the reaction products is exceeded and new phases appear *via* the solution–precipitation path. The assumption of the solution–precipitation path for the formation of new phases implies the existence of a dynamic situation within the structure of the cathode. Factors that contribute to this dynamic situation are the degree of local supersaturation, the rate of mass transport, and the rate of precipitation and growth of crystallites. The observation of a variety of growth forms of LiCl, Fig. 7(a) - (d), produced by the same overall electrochemical process gives rise to the question: What determines the shape of the growing crystallites?

The question of growth stability and shape preservation during growth has been examined extensively [13 - 16]. It is generally agreed that the shape of growing crystallites is affected by two factors: mass transport and interfacial processes. Thus, even if a particle at its critical size were spherical,

deformation of its shape would occur when its size exceeds 7 times its critical value, as required by the Mullins–Sekerka theory [13]. The shape of the growing particle reflects the anisotropy of interfacial processes in conjunction with transport, with the former being effective before the bulk diffusion becomes the rate determining step (rds).

A convenient method to assess the degree of involvement of elementary processes is the SEM examination of spent electrodes. This examination reveals a variety of morphological forms, *e.g.*, well defined cubic crystallites, 1 - 2 μm in size, Fig. 7(a), elongated plate-like growth, 3 - 4 μm in size, Fig. 7(b), a mixture of cubic elongated crystallites, Fig. 7(c), and finally, large, plate-like, fused crystals, approximately 100 μm long, covered with a mossy deposit of submicron size, Fig. 7(d).

The well defined cubic form implies that the growth process has occurred in a free space and in the absence of concentration gradients. The uniform size suggests that Oswald ripening was operative, leading to the homogenization of crystallite size [17], *i.e.*, the local current density was low and the degree of supersaturation was relatively constant. Plate-like crystals shown in Fig. 7(b) exhibit preferred growth directions, thereby suggesting growth in free space assisted by concentration gradients. Again, their uniform size indicates Ostwald ripening. Figure 7(c) illustrates yet another growth form. Here, the submicron size particles rest over well defined cubic ones. By contrast, fused, plate-like aggregates, shown in Fig. 7(d), indicate an interference in the growth process by mechanical constraints. The formation of a mossy growth is attributed to a high degree of local supersaturation and the presence of concentration gradients. Such conditions may be created by high charge transfer density and convective flow of electrolyte.

In addition to the formation and growth of LiCl crystals, elemental sulfur is also found. The elemental sulfur is uniformly distributed throughout the electrode structure, provided that there are no cracks or voids. In the presence of these defects, sulfur found in those defects appears either in the form of a film or in the form of crystallites, Fig. 8(a) and (b), respectively. The sulfur film is frequently found in voids resulting from inadequate contact between the bipolar plate and the electrode matrix.

Current distribution

The evolution of current density profiles as a function of discharge time was derived from SEM examination and EDAX analysis of spent electrodes using an Al internal standard. The results are shown in Fig. 9(a) - (d) for 1/4, 1/2, 3/4 and full discharge where Cl/Al ratios are plotted against the distance from the bipolar plate, curve 1. The distribution of S is also shown, curve 3. It is noted that there is no direct correspondence between Cl and S profiles, curves 1 and 3, respectively. This would imply that precipitation of sulfur occurs at a later time than LiCl, thus exhibiting a levelling effect attributed to transport within the electrode matrix.

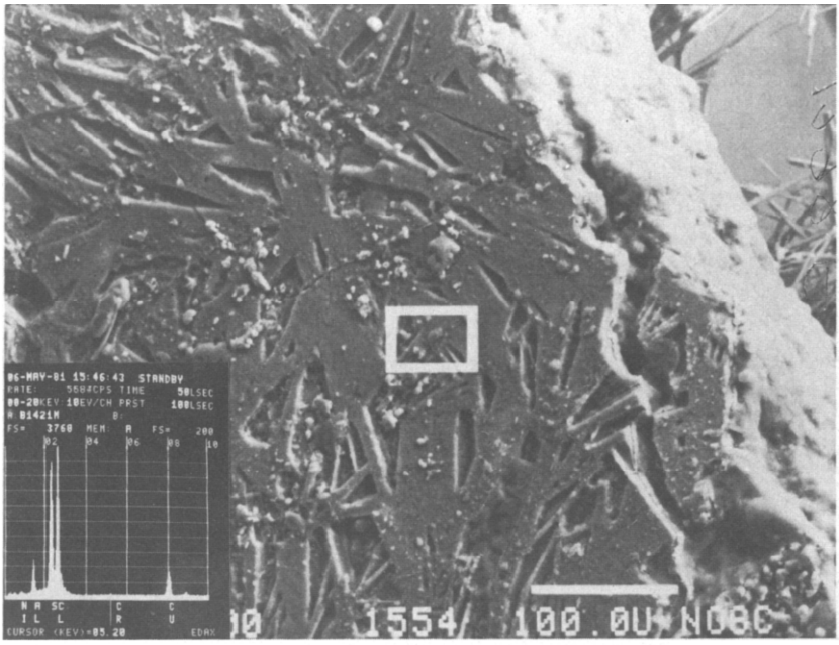

(a)

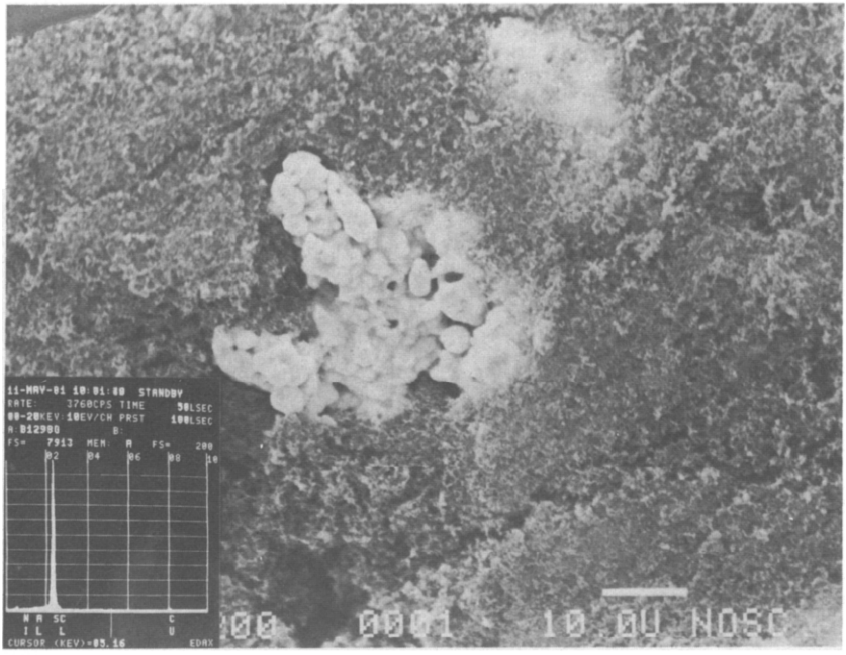

(b)

Fig. 8. Sulfur precipitation in defective electrodes. (a) sulfur film formed between bipolar plate and porous matrix; (b) sulfur crystals found in electrode matrix. Results of EDAX analysis shown in lower left corner. Electrolyte, 1.9M $LiAlCl_4$ + 0.3M $AlCl_3$ in $SOCl_2$. Temperature, room. Discharge CD, 75 mA cm^{-2}.

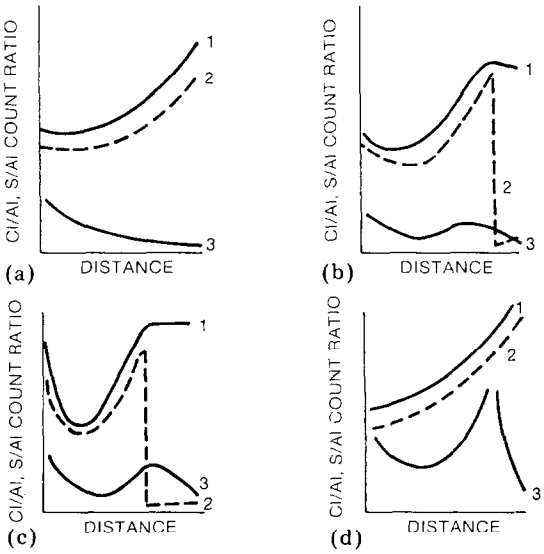

Fig. 9. Charge transfer distribution derived from EDAX analysis. Upper curve showing Cl/Al ratio, curve 1; lower curve showing S/Al ratio, curve 3; broken line indicates current density distribution, curve 2. Data are qualitative. Electrolyte, 1.9M $LiAlCl_4$ + 0.3M $AlCl_3$ in $SOCl_2$. Temperature, room. Discharge CD, 80 mA cm^{-2}. Cathode thickness, 0.024 cm.

Admittedly, results and their interpretation are qualitative, they nevertheless clearly indicate that initially, the reduction of $SOCl_2$ takes place in the electrode segment facing the negative. The highly nonlinear distribution indicates that initially the resistance in the electrolyte phase controls the distribution of reaction intensity. This is an expected result since the resistance of the electrode matrix is much less than that of the electrolyte phase.

The charge transfer profile changes with time, curve 2; the reaction zone penetrates deeper into the electrode structure, Fig. 9(b). This penetration can be attributed to either deactivation of reaction sites, to an increase in the resistance of the electrode matrix, or both. At present there is not sufficiently strong evidence that would allow us to ascribe deactivation to any particular process or specific reaction product. The observed minima in the CD profiles, Fig. 9(b) and (c) are characteristic of the position dependent resistance in both electrolyte and electrode matrix. Here, however, mass transport can play a dominant role in the development of minima. Toward the end of battery discharge, the rds reverts to the electrolyte phase and, likely, electrode performance is governed solely by mass transport, Fig. 9(d).

Electrode expansion

Expansion of the positive electrode during discharge was observed by Marincic [1]. He has attributed this to the precipitation of insoluble discharge products in the pore structure of the electrode. We shall extend his treatment by a quantitative discussion of this phenomenon.

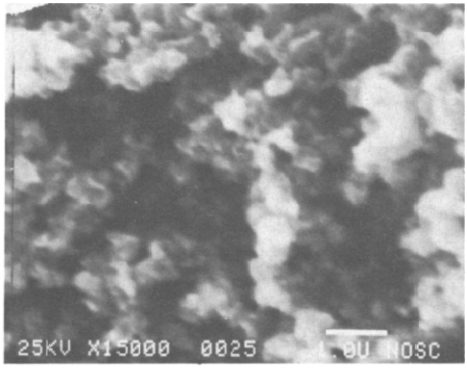

(a)

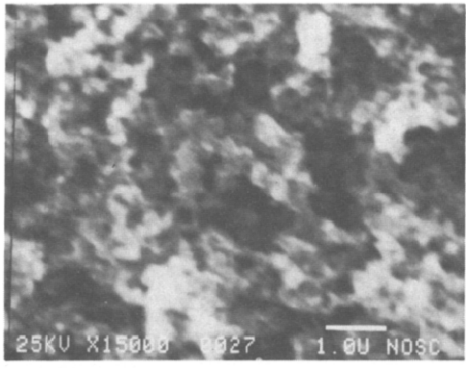

(b)

Fig. 10. Illustration of electrode matrix expansion. (a) Electrode section facing bulk electrolyte; (b) center section of electrode matrix. Electrolyte, 1.9M $LiAlCl_4$ + 0.3M $AlCl_3$ in $SOCl_2$. Temperature, room. Discharge CD, 80 mA cm^{-2}. Cathode thickness, 0.024 cm.

A standard electrode with a surface density of 9 mg/cm^2 was discharged for 1 min at 75 mA/cm^2, *i.e.*, to about 12% of its capacity. After discharge, the reaction products were extracted with distilled thionyl chloride followed by a rinse with de-ionized water. The SEM examination clearly revealed electrode expansion in the region facing the negative electrode where the reaction zone was located, *cf.* Fig. 10. The interior of the electrode showed less separation between individual carbon particles.

The swelling of electrodes in the course of battery discharge may be explained as follows: The Gibbs–Thompson equation, eqn. (1), states that a relationship exists between pore size and critical supersaturation, leading to nucleation and growth of a new phase.

$$c(r) = c(\infty) \exp(2\sigma V_m / RTr) \quad (1)$$

where $c(r)$ and $c(\infty)$ are pore radius dependent concentrations, σ is the surface tension, V_m is the molar volume of the new phase and r is the pore radius (R and T have their usual meaning). Since the reaction occurs within an elec-

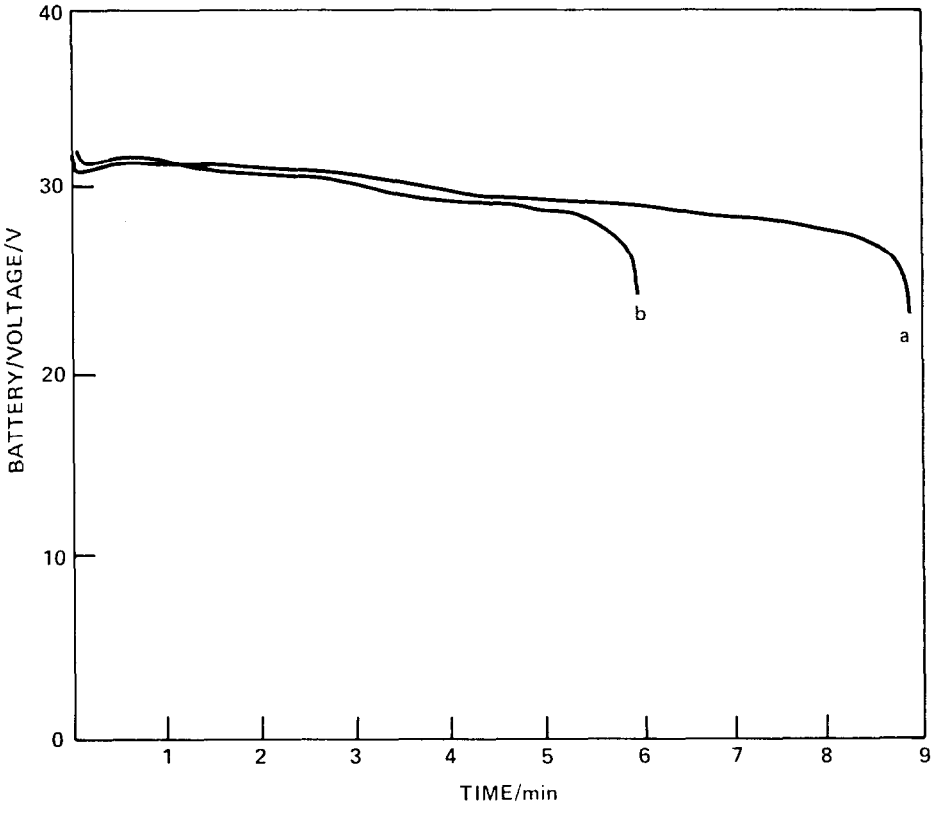

Fig. 11. Effect of electrode expansion on battery capacity. (a) With space for expansion provided; (b) without available space for expansion.

trode structure with a pore size of the order of 10^{-5} cm, the critical supersaturation of LiCl is greater than that in the bulk solution. On the other hand, this pore size does not impede mass transport. Consequently, a concentration gradient is established at the pore mouth and this leads to initial nucleation and growth of crystallites at the pore mouth in the bulk electrolyte. The precipitated LiCl reduces the area available for transport, thus restricting it and promoting nucleation and growth within the pore. Growth now takes place within the mechanical constraints of the pore, and exerts a pressure, p, given in eqn. (2).

$$p = \frac{RT}{V_m} \ln \frac{c(r)}{c(\infty)} \tag{2}$$

which causes separation of individual grains as illustrated in Fig. 10, resulting in electrode swelling.

From a practical point of view electrode swelling is an important aspect of $Li/SOCl_2$ battery operation. Space must be provided for electrode expansion if full capacity is to be delivered. This is illustrated in Fig. 11 where two

identical 10-cell batteries, one of which was provided with space for electrode expansion and the other was not, were discharged under identical conditions with a current density of 75 mA cm^{-2}.

Because of the change in critical supersaturation with pore size, voids greater than 10^{-5} cm should be avoided in the area of the cathode–bipolar plate junction. Failure to do so may result in the preferential deposition of elemental sulfur in this region (Fig. 8), resulting in greatly increased contact resistance and, consequently, greatly increased cell polarization.

Conclusions

(1) SEM examination of partially and/or totally discharged cathodes may provide information on local conditions governing the growth form of LiCl.

(2) When combined with the EDAX investigation, it leads to the construction of reaction intensity profiles as a function of discharge capacity.

(3) Electrode swelling promotes the high discharge rate operation of Li/$SOCl_2$ cells and batteries and full capacity utilization.

(4) Uniformity of pore size with the positive electrode should be maintained to avoid preferential deposition of reaction products which may lead to cell failure.

Acknowledgements

This work was performed in support of the Advanced Lithium Battery Program. The financial support was provided by Naval Sea Systems Command, Code 63R-33 and PMS-406.

References

1 N. Marincic, *J. Appl. Electrochem., 5* (1975) 313; *6* (1976) 51; *6* (1976) 263; *6* (1976) 463.
2 A. N. Dey, *J. Electrochem. Soc., 123* (1976) 1262.
3 J. A. Christopulos and S. Gilman, *Proc. Intersociety Energy Conversion* (IEEE publisher), *Newark, DE, 1975.*
4 K. A. Klinedinst and M. J. Domeniconi, *J. Electrochem. Soc., 127* (1979) 539.
5 P. Bro and A. N. Dey, *Ext. Abstr. #23, Electrochem. Soc. Fall Meeting, Las Vegas, NE, 17 - 22 October, 1976,* Electrochemical Soc. Inc.
6 L. R. Giattino, *U.S. Pat. No. 4,167,608* (1979).
7 K. A. Klinedinst, *J. Electrochem. Soc., 128* (1981) 2507.
8 H. V. Venkatasetty, *U.S. Pat. No. 4,279,973* (1981).
9 T. Katan and S. Szpak, *Ext. Abstr., Electrochem. Soc. Fall Meeting, New York, NY, 1974.*
10 W. K. Behl, *J. Electrochem. Soc., 128* (1981) 939.
11 E. Yeager, *J. Electrochem. Soc., 128* (1981) 160C.
12 J. Zagal, P. Bindra and E. Yeager, *J. Electrochem. Soc., 127* (1980) 1506.
13 W. W. Mullins and R. F. Sekerka, *J. Appl. Phys., 34* (1963) 323.
14 A. A. Chernov, *Sov. Phys. — Crystallog.,* 7 (1963) 728; *8* (1963) 63; *8* (1964) 401.
15 S. K. Chem, H. H. Reimer and M. Kahlweit, *J. Cryst. Growth, 32* (1976) 303.
16 H. Muller-Krumbhaar, T. W. Burkhardt and D. M. Kroll, *J. Cryst. Growth, 38* (1977) 13.
17 F. S. Ham, *J. Phys. Chem. Solids, 6* (1958) 335.